

Airborne Measurements of Surface Anisotropy

S. C. Tsay

*Climate & Radiation Branch
NASA-Goddard Space Flight Center
Greenbelt, Maryland*

M. D. King

*Earth Sciences Directorate
NASA-Goddard Space Flight Center
Greenbelt, Maryland*

G. T. Arnold and J. Y. Li

*Space Applications Corporation
Vienna, Virginia*

Introduction

Surface spectral bidirectional reflectance is a major parameter of interest to the biospheric sciences, remote sensing, and global change communities. For example, the pronounced reflectance peak at the back scattering range of vegetated surfaces, known as the “hot spot” or “opposition surge” (cf. Hapke 1993), is found to be closely related to the state of several biophysical and physical parameters (e.g., Pinty and Verstraete 1991). The surface bidirectional reflectance also plays a crucial role in the radiative energy balance, since it is required to determine 1) the spectral and spectrally integrated albedo (e.g., Ranson et al. 1991), and 2) the top-of-the-atmosphere angular distribution of the radiance field (e.g., Hapke 1993). It is common practice to assume a Lambertian (isotropic) surface in general circulation models or global climate models (GCMs), and/or to estimate albedo from satellite/aircraft measurements close to nadir (Barnsley et al. 1994, and references therein). The Lambertian assumption is invalid for most natural surfaces and estimations of albedo from nadir measurements have been shown to be in error by as much as 45% (e.g., Kimes et al. 1987). In turn, a vital piece of information for climate studies and remote sensing applications is the anisotropy of the surface reflectance.

Instruments best designed for measuring surface bidirectional reflectance should meet the following two requirements: 1) provide multiple viewing angle measurements in a short period of time to minimize the effects of changing source and target conditions, and 2) simultaneously measure the downwelling radiance from the source and upwelling radiance from the target. During SCAR-B (Smoke, Clouds, And Radiation - Brazil, August-September 1995), one such multispectral scanning radiometer flew aboard the University of Washington’s Convair C-131A aircraft and

acquired data of spectral bidirectional reflectance over a large area in Brazil under various environmental conditions.

Definitions and Considerations

According to the National Bureau of Standards, the spectral bidirectional reflectance distribution function (Nicodemus et al. 1977), ρ_λ , is defined as

$$\rho_\lambda(\theta_r, \phi_r; \theta_i, \phi_i) = \frac{dI_\lambda(\theta_r, \phi_r; \theta_i, \phi_i)}{dF_\lambda(\theta_i, \phi_i)} \quad (1)$$

which is a ratio of two derivatives; F_λ is the collimated irradiance illuminating at zenith angle θ_i and azimuth angle ϕ_i ; and I_λ is the corresponding reflected radiance at angles θ_r and ϕ_r . In Eq. (1), ρ_λ is in units of sr^{-1} . Theoretically, the principle of reciprocity, $\rho_\lambda(\theta_r, \phi_r; \theta_i, \phi_i) = \rho_\lambda(\theta_i, \phi_i; \theta_r, \phi_r)$, is well satisfied (e.g., Hapke 1993). However, in dealing with actual measurements and applications, there are many factors that need be considered to appropriately describe the distribution of bidirectional reflectance.

Measurements from radiometric instrumentation are always confined within an instantaneous field of view (IFOV)—a finite solid angle defining the incident and viewing directions, not a derivative. Added to this is that under natural conditions photon scattering and/or absorption may occur before photons are received by the instrument sensors. In turn, additional amounts of diffuse radiation may be detected by the sensors. Thus, Eq. (1) is not practical in defining measurements of surface anisotropy. In addition, depending on the properties of the intervening media (e.g., concentration and optical characteristics of molecules and particles along slant paths) and the state of the reflecting surface (e.g., leaf orientation, wetness, etc.), the

bidirectional reflectance pairs measured at different times may not obey the principle of reciprocity. To characterize the surface anisotropy from spectral measurements, we adopt the definition, commonly used in the atmospheric radiation community (e.g., van de Hulst 1980), of bidirectional reflection function (BRF, R_λ) given as

$$R_\lambda(\theta, \theta_0, \phi) = \frac{\pi I_\lambda(\theta, \theta_0, \phi)}{\mu_0 F_\lambda} \quad (2)$$

where θ and θ_0 are respectively the viewing and illumination zenith angles; ϕ , the azimuth angle between the viewing and illumination directions; and $\mu_0 = \cos \theta_0$. Thus, the BRF in Eq. (2) is dimensionless and directly normalized to the reference illumination irradiance. This avoids the potential problems that the illumination source may not be covered entirely by the instrument IFOV and/or not be captured fully by the viewing geometry, as well as to prevent possible signal saturation due to instrument dynamical range. Similarly, for the spectral albedo, r_λ , radiances received by the detector from all viewing directions/solid angles are integrated (or summed up for all IFOVs). By substituting Eq. (2), it becomes

$$r_\lambda(\theta_0) = \frac{1}{\pi} \int_0^{2\pi} \int_0^{\pi/2} R_\lambda(\theta, \theta_0, \phi) \cos \theta \sin \theta d\theta d\phi \quad (3)$$

$$\equiv \frac{1}{\mu_0 F_\lambda} \left[\sum_{i=1}^M \sum_{j=1}^N I_\lambda(\theta_i, \theta_0, \phi_j) \cos \theta_i \sin \theta_i \Delta\theta_i \Delta\phi_j \right]$$

where (i, j) are respectively the indices of (θ , ϕ) for discretization (M, N terms) over the hemisphere.

Instrumentation and Data Collection

During SCAR-B, measurements of surface bidirectional reflectance were acquired by using a multispectral, scanning radiometer—the Cloud Absorption Radiometer (CAR), which was designed and built at the NASA Goddard Space Flight Center (cf. King et al. 1986 for details). In brief, the CAR, mounted in the nose of the University of Washington's C-131A research aircraft, provides radiometric measurements at 13 discrete wavelengths between 0.3 μm and 2.3 μm . Figure 1 shows the clear-sky atmospheric transmittance and relative positions of the CAR channels. A midlatitude summer atmosphere (Anderson et al. 1986) was used to compute the transmittance from the top of the atmosphere to 1 km height. As shown in Figure 1, all of the CAR channels were carefully selected to minimize the effects of gaseous absorption, except for the UV-B channel where ozone absorption is desired. They are centered at wavelengths of 0.307 (or 0.754, interchangeable

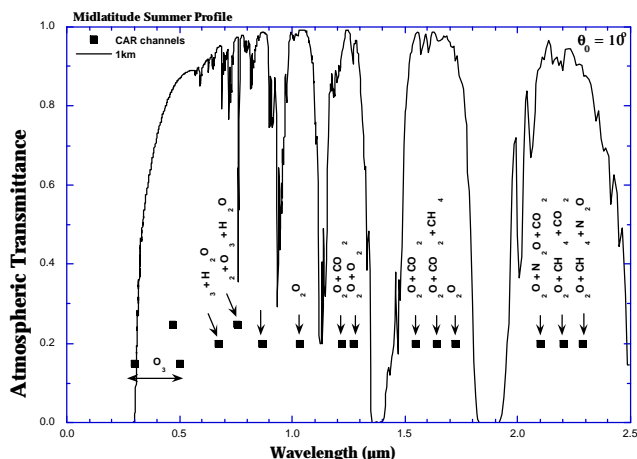


Figure 1. Clear-sky transmittance and the relative positions of CAR channels (see text for details).

but not used in SCAR-B), 0.472 (or 0.507), 0.675, 0.869, 1.038, 1.219, 1.271, 1.552, 1.643, 1.725, 2.099, 2.207, and 2.303 μm . The CAR channels at the visible wavelengths are affected weakly by ozone absorption (i.e., Chappuis band) and more by Rayleigh scattering, resulting in about 3% to 12% reduction in atmospheric transmittance. However, both of these effects are well known and relatively easy to correct. The 0.869 μm and 1.038 μm bands are the cleanest window channels, where both Rayleigh scattering and ozone absorption are largely negligible. In the shortwave-infrared channels, water vapor and trace gas absorption can produce about a 2% to 8% reduction in atmospheric transmittance.

The optical system of the CAR is non-dispersive, being composed of a complex configuration of dichroic beam splitters and narrowband interference filters. The filter wheel contains optical channels 8 through 13 (i.e., 1.552 μm to 2.303 μm), and can be locked at a particular channel or rotated to measure a new wavelength interval after a preset number of scans. In general, the bandwidth of the CAR channels is about 20 nm, except for the filter wheel channels where $\Delta\lambda \bullet 40$ nm. With this configuration, the first seven channels are continuously and simultaneously sampled, while the eighth registered channel is selected from among the six channels on the filter wheel. To allow for the large variations in absolute magnitude of the radiance arising as a function of optical properties of the target and, especially, the solar zenith angle, the CAR provides for seven manual gain selections that apply a uniform gain adjustment to all eight electrical channels simultaneously. This manual gain setting, which permits greater flexibility in field operations, is output to the data system for retrieval.

Viewing with an IFOV of 1°, the CAR scans in a vertical plane on the right-hand side of the aircraft from 5° before

zenith to 5° past nadir (190° aperture); thereby permitting observations of both the zenith and nadir radiances to be obtained with as much as a 5° aircraft roll, an angle that is measured simultaneously with a gyroscope aboard the aircraft. In addition, by rotating the instrument 90° around the aircraft's principal axis, the CAR can also be used as a downward looking, cross-track imager. This imaging capability was successfully demonstrated during SCAR-B.

By definition [Eq. (2)], the BRF describes the angular distribution of reflected radiances from an element of surface area, in terms of which the setup of instrumentation should resemble a sensor with a goniometer (cf. e.g., Figure 1 of Perovich 1994) looking at a particular area with all selected viewing angles. Although the goniometer approach, as frequently adopted by geologists, provides a more precise bidirectional geometry, it suffers from sampling inefficiency for most remote sensing applications. With such deployment, the spatial resolution is generally far less than one meter due to the size limitation of the goniometer, and the measurements are susceptible to the fine variation of specific properties of the targeted surface area. Hence, a large volume of samples obtained under identical source and surface conditions is required. For airborne measurements, the goniometer-like sampling strategy is even more difficult to implement, mainly due to the requirement of a long observation period. Alternatively, if the average conditions of the targeted surface area are nearly homogeneous, the approach depicted in Figure 2 should provide the most mobile and efficient means for airborne measurements of surface bidirectional reflectance.

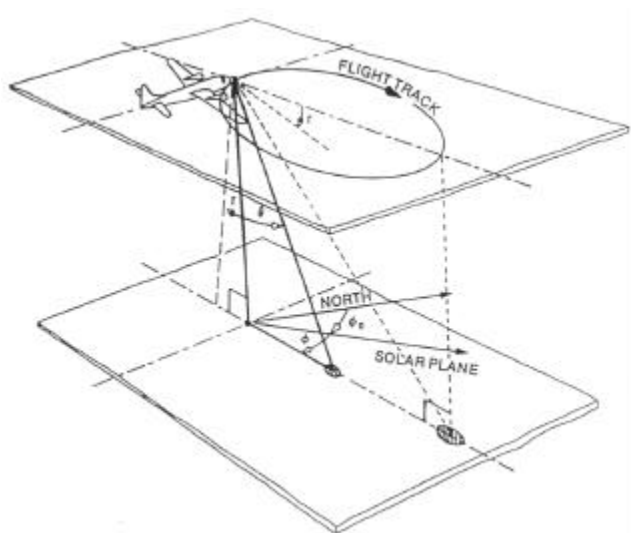


Figure 2. Schematic illustration of a clockwise circular flight track for measuring both the reflected and transmitted solar radiation.

In Figure 2, the operational specifications for the CAR in measuring the surface bidirectional reflectance are shown. The average speed of the C-131A is about 80 m s^{-1} , which results in a minimum circle of about 3 km in diameter at a comfortable roll angle of 20° in about 2 minutes. At an altitude of 600 m above the targeted surface area and 1° IFOV, the pixel resolution is about 10 m at nadir and about 270 m at an 80° viewing angle from the CAR. During the SCAR-B campaign, four types of surface bidirectional reflectance were obtained under this flight track: cerrado, dense forest, dense smoke layer, and reservoir water.

Figure 3 shows an example of CAR measurements in a time series of spectral (e.g., $1.271 \mu\text{m}$) imagery for Flight 1701 (13:21 to 13:58 UT September 6, 1995) near Porto Velho, Brazil. The upper half of the image strip (0° to 90° , 0° for zenith) denotes the measurements of sky radiance and the lower half (90° to 180° , 180° for nadir) surface reflected radiances. As demonstrated by the $1.271 \mu\text{m}$ channel, the vegetated surface appears bright and the effect of aerosol scattering is reduced. At the beginning of the image, the CAR was scanning in the principal plane, where the solar disk (bright spot in the upper part) and the corresponding specular reflection from the river water are clearly seen. Since the image was not presented in a proper aspect ratio, the solar disk appears as an oval shape. The black rectangular boxes around the nadir viewing direction were the missing data due to sharp turning of aircraft (banking to the left with roll angle $> 5^\circ$). The lower half of the last 12 minutes of the image demonstrates the measurements of surface bidirectional reflectance, as depicted in Figure 2. Replicated observations (multiple circular orbits) were acquired for every selected surface.

Results

The fundamental assumption involved in reconstructing a bidirectional reflectance from CAR measurements is the homogeneity of the targeted surface area. By selecting the targets carefully, the approach depicted in Figure 2 should prove the most mobile and efficient means of measuring surface bidirectional reflectance. During SCAR-B, the spectral BRF measurements for four types of surfaces were selected and obtained in five CAR flight missions. Here, we present results of cerrado, acquired in Goias, north of Brasilia, under nearly clear-sky conditions, from 18:51 UTC to 19:02 UTC on August 18, 1995 (Flight 1689) and leave the other cases in the work of Tsay et al. (1998).

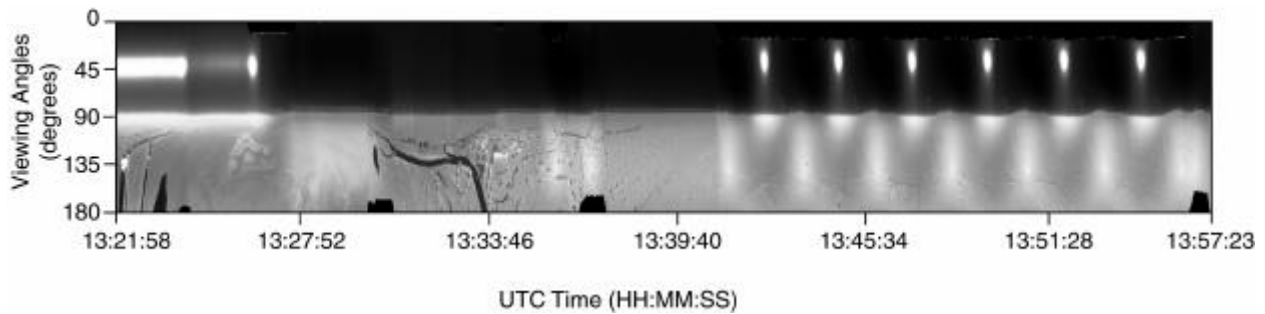


Figure 3. Example of CAR measurements ($1.271 \mu\text{m}$) in a time series (13:21 - 13:58 UT) on September 6, 1995 during SCAR-B (see text for details).

Figure 4 shows a photograph of cerrado, taken from the University of Washington's C-131A aircraft around the time the spectral measurements of surface bidirectional reflectance were obtained. Cerrado (savannah) is mainly composed of scrub-like vegetation, in which the ground cover is uniform but not very dense. Five circular orbits were made to produce replicated BRF observations in order to average out surface inhomogeneity. For the first three orbits the filter wheel channel was locked at the $1.643 \mu\text{m}$ band, and the last two orbits at the $2.207 \mu\text{m}$ band. Within this observational period (~ 11 min), the solar zenith angle varied from 59.07° to 61.73° . Because less data were taken for the filter wheel channels, their variations in solar zenith angle were smaller. The background aerosol loadings were reported to be very low by the C-131A meteorologist and the retrieved aerosol optical thickness at $0.67 \mu\text{m}$ channel from the sunphotometer was less than 0.1 in the vicinity of Brasilia.



Figure 4. Photograph of cerrado taken from the University of Washington's C-131A aircraft. (For a color version of this figure, please see http://www.arm.gov/docs/documents/technical/conf_9803/tsay-98.pdf.)

Figure 5 demonstrates the spectral BRF measured over cerrado. In all polar plots, zenith is represented as radial distance from the center, azimuth as length of the arc on the respective zenith circle. The principal plane resides in the 0° to 180° azimuthal plane with the sun located in the 180° azimuth direction. With this definition, the upper half of the circles represents forward scattering and the lower half represents back scattering, with the anti-solar direction at $\theta_0 \bullet 60^\circ$, shown as a white spot in Figure 5a. Two striking features appear clearly in Figure 5: a highly symmetric pattern, and a strong reflection in the back scattering direction. Although the averaged BRF data from all circles have further smoothed and symmetrized the bidirectional reflectance pattern, yielding good statistics in representing cerrado, BRF data from an individual circle are not much different from one another. The observed strong back scattering signal, peaked at $\sim 60^\circ$ zenith angle in the principal plane at $\phi = 180^\circ$, is known as the "hot spot" or "opposition surge" (Hapke 1993). For this case, the reflection functions have values near or close to 0.6 in the $0.869 \mu\text{m}$ to $1.643 \mu\text{m}$ region. Apparently, the spectral and angular information, such as the amplitude and width of the hot spot feature, are closely related to the specific biophysical parameters (e.g., leaf size, shape, density, etc.). The surface spectral anisotropy retains similar patterns, but becomes less pronounced in the visible region due to chlorophyll absorption as well as strong light scattering by the atmosphere. This is clearly seen in the blue channel ($0.472 \mu\text{m}$), in which the range of back scattering peak is broadened.

To investigate the detailed angular distribution of BRF, Figure 6 shows the spectral dependence of the reflection function along the principal plane. The amplitude and angular width of the hot spot for cerrado, located at $\sim 60^\circ$ (a few degrees off at $2.207 \mu\text{m}$ due to time differences), reveals strong spectral dependence. In the $0.869 \mu\text{m}$ to $1.271 \mu\text{m}$ range, the shape of the hot spot is spiky; while its amplitude is reduced and becomes broader towards longer (e.g., $2.207 \mu\text{m}$) or shorter (e.g., $0.675 \mu\text{m}$) wavelengths. A

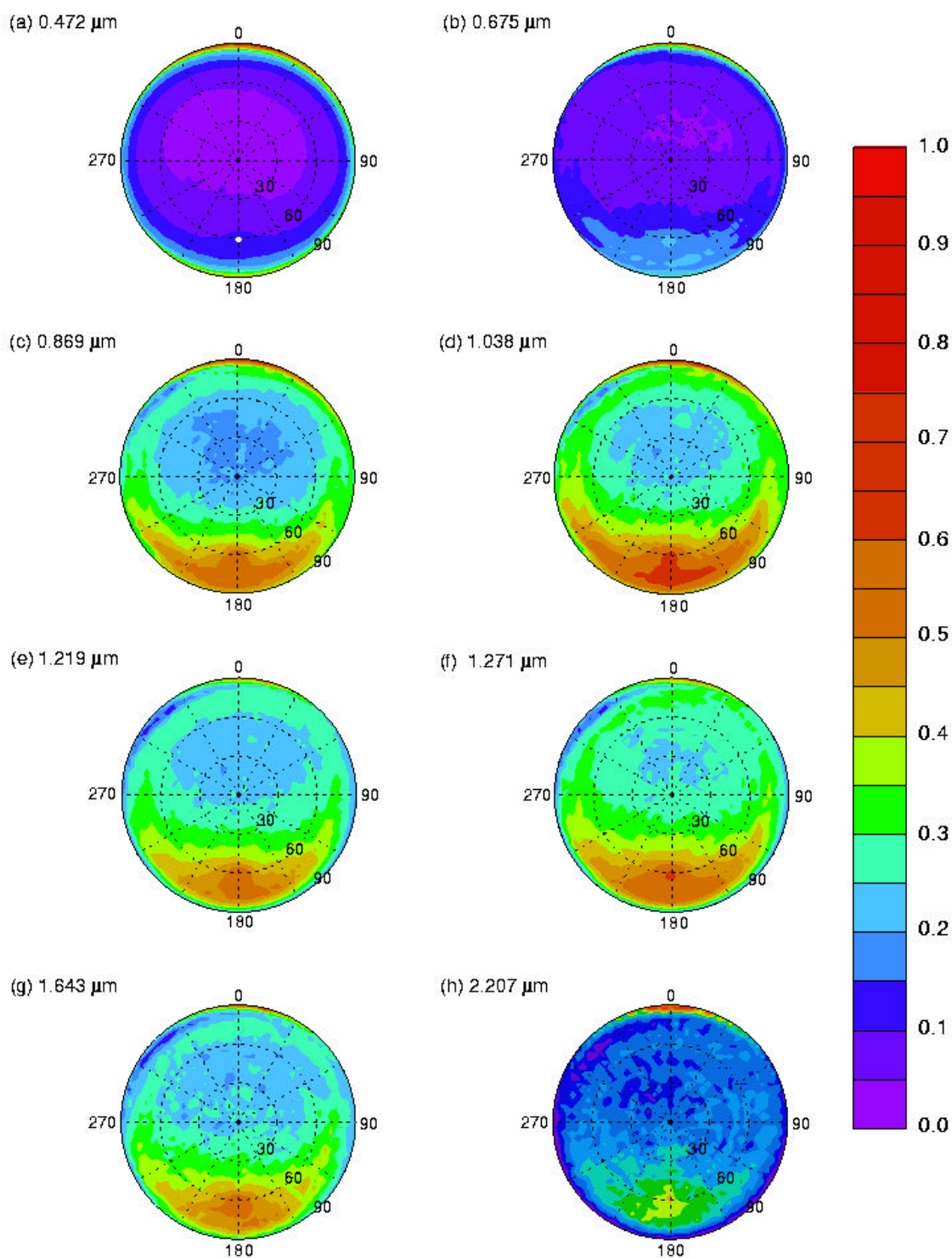


Figure 5. Spectral measurements of surface bidirectional reflectance over cerrado on August 18, 1995, during SCAR-B. The location of the anti-solar point at $\theta = 60^\circ$ and $\phi = 180^\circ$ is indicated in (a). (For a color version of this figure, please see http://www.arm.gov/docs/documents/technical/conf_9803/tsay-98.pdf.)

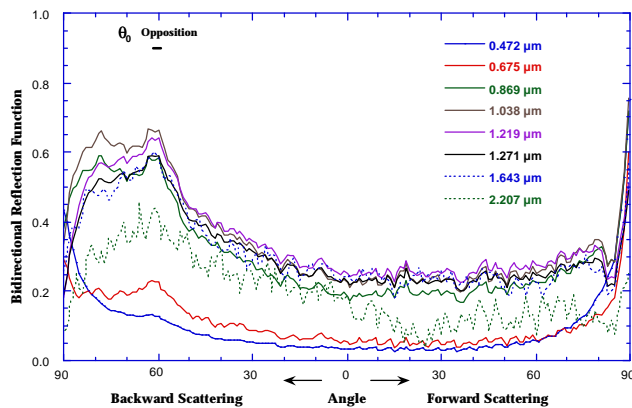


Figure 6. Angular distribution of BRF in the principal plane for cerrado during SCAR-B. (For a color version of this figure, please see http://www.arm.gov/docs/documents/technical/conf_9803/tsay-98.pdf.)

secondary peak of back scattering exists near $\theta \bullet 75^\circ$ for the 0.869 μm to 1.271 μm channels, and is greatly suppressed at the 0.675 μm , 1.643 μm , and 2.207 μm channels. This phenomenon may be related to the multiple scattering among leaves with particular leaf angle distributions. Reflection functions for all channels show limb darkening in the back scattering horizon direction, except for the blue (0.472 μm) channel where Rayleigh scattering becomes dominant. In the forward scattering portion, limb brightening is clearly seen at the horizon for all channels. Whether these limb darkening and brightening features are solely (or in part) due to atmospheric effect or surface BRF itself remain to be explored through modeling.

References

- Anderson, G. P., S. A. Clough, F. X. Kneizys, J. H. Chetwynd, and E. P. Shettle, 1986: *AFGL atmospheric constituent profiles (0-120 km)*, AFGL-TR-86-0110.
- Barnsley, M. J., 1984: Effect of off-nadir view angles on the detected spectral response of vegetation canopies. *Int. J. Remote Sens.*, **5**, 715-728.
- Hapke, B., 1993: *Theory of Reflectance and Emittance Spectroscopy*, Cambridge University Press, 455 pp.
- Kimes, D. S., P. J. Sellers, and D. J. Diner, 1987: Extraction of spectral hemispherical reflectance (albedo) of surface from nadir and directional reflectance data. *Int. J. Remote Sens.*, **8**, 1727-1746.
- King, M. D., M. G. Strange, P. Leone and L. R. Blaine, 1986: Multiwavelength scanning radiometer for airborne measurements of scattered radiation within clouds. *J. Atmos. Oceanic Tech.*, **3**, 513-522.
- Nicodemus, F. E., J. C. Richmond, J. J. Hsia, I. W. Ginsberg, and T. Limperis, 1977: Geometrical considerations and nomenclature for reflectance. *Natl. Bur. Stand. Monogr.*, **160**, U.S. Govt. Print. Off., Washington, D.C., 52 pp.
- Perovich, D. K., 1994: Light reflection from sea ice during the onset of melt. *J. Geophys. Res.*, **99**, 3351-3359.
- Pinty, B., and M. M. Verstraete, 1991: Extracting information on surface properties from bidirectional reflectance measurements. *J. Geophys. Res.*, **96**, 2865-2874.
- Ranson, K. J., J. R. Irons, and C. S. T. Daughtry, 1991: Surface albedo from bidirectional reflectance. *Remote Sens. Environ.*, **35**, 201-211.
- Tsay, S. C., M. D. King, G. T. Arnold, and J. Y. Li, 1998: Airborne spectral measurements of surface anisotropy during SCAR-B. *J. Geophys. Res.*, **103**, in press.
- van de Hulst, H. C., 1980: Multiple light scattering: tables, formulas, and applications. Academic Press, 739 pp.